Available online at www.sciencedirect.com
ScienceDirect
Acta Materialia 59 (2011) 5574–5583
Acta MATERIALIA
www.elsevier.com/locate/actamat

Modeling of enhanced electrocaloric effect above the Curie temperature in relaxor ferroelectrics

Y.P. Shi, A.K. Soh *

Department of Mechanical Engineering, The University of Hong Kong, Hong Kong

Received 12 January 2011; received in revised form 16 May 2011; accepted 16 May 2011
Available online 12 June 2011

Abstract

The electrocaloric (EC) effect offers promise as a means to realize solid-state refrigeration, which requires EC materials possessing a pronounced pyroelectric effect over a broad temperature range. Pauli's master equation is adopted to investigate the recently observed phenomenon of enhanced EC effect above the Curie temperature in relaxor ferroelectrics. The proposed approach allows the EC coefficient to be determined within the framework of classic Landau–Ginzburg–Devonshire thermodynamics and the Maxwell relation, taking into account both the depolarization effect and dielectric permittivity dispersion based on the concept of superparaelectricity and the nanopolar region. We analyze three contributions of the EC effect: temperature-dependent dielectric dispersion, intrinsic pyroelectric effect and enhanced dielectric stiffness. The maximum EC coefficient is determined through the derivatives of the three components with respect to temperature. The proposed approach, in which the evolution of polarization correlation length is accounted for, cannot only provide a microscopic explanation for the thermally driven enhancement of EC responses, but also improves upon the existing models for estimating the EC effect in paraelectric phase of relaxors. Finally, some potential approaches for engineering the enhancement of EC coefficient are also suggested.

Keywords: Electrocaloric effect; Relaxor ferroelectrics; Dielectric stiffness enhancement; Pauli's master equation; Phenomenological theory

1. Introduction

The electrocaloric (EC) effect, which is the physical inverse of the pyroelectric effect, refers to the adiabatic temperature change induced by reversibly isoentropic application of an electric field in polarizable materials. This topic has received renewed research interests inspired by the recently observed enormous EC responses in relaxor ferroelectric single crystals [1] and polymers [2] due to their ultrahigh breakdown fields. The strength of the EC effect is characterized by the so-called EC coefficient, χ, which is defined as the ratio of the adiabatic temperature rise ΔT to the corresponding increment of external electric field ΔE. Owing to its intrinsic advantages in terms of energy efficiency [3] and environmental friendliness [4], the EC effect observed in a large number of relaxor ferroelectrics and ferroelectric polymers has been recognized as a promising alternative [2] to the existing Peltier-effect-based technologies used in solid-state cooling devices [3]. However, apart from very limited direct measurements of the resultant EC temperature change [5,6], the existing studies on the temperature- and electric-field-dependent EC effect have so far been limited to first-principles atomistic simulations [7,8] or solely numerical predictions based on the Maxwell relation [10–12] and phenomenological theories [6,13–16]. In particular, the Maxwell relation correlates the EC coefficient (χ) and pyroelectric coefficient (γ), as follows:

$$\chi = -T\gamma_E/C_E \tag{1}$$

where T and E denote the absolute temperature and the magnitude of the applied electric field, respectively, and C_E is the volumetric specific heat at constant E. Note that

* Corresponding author. Tel.: +852 28598061; fax: +852 28585415.
E-mail address: aksoh@hkucc.hku.hk (A.K. Soh).

1359-6454/$36.00 © 2011 Acta Materialia Inc. Published by Elsevier Ltd. All rights reserved.
doi:10.1016/j.actamat.2011.05.030

this equation is valid under the condition of constant entropy. It can be inferred from Eq. (1) that, in order to qualify as a feasible candidate for applications in commercial cooling devices, EC materials should possess a pronounced pyroelectric effect over a relatively broad temperature range [3]. This is because both changes in isothermal entropy and adiabatic temperature are in practice required to maintain significantly high levels of EC responses during cyclic cooling so that the desired cooling power can be produced.

The Landau–Ginzburg–Devonshire (LGD) theory has also been widely employed to predict the average EC adiabatic temperature change as follows:

$$\Delta T = -\kappa T P^2 / C_E \tag{2}$$

where P is an order parameter in the form of electric polarization, and κ is often defined as a temperature-independent dielectric stiffness [3,13], which is inversely proportional to the Curie–Weiss constant [17]. Obviously, LGD theory indicates that both the Curie temperature T_C, at which the EC effect accompanied by ferroelectric phase transition [1,10] or dipolar ordering–disordering transition [9,14] is strongest, and the dielectric stiffness could affect ΔT, whereas only κ was found to have significant effect on the EC isothermal entropy change (ΔS) [3]. This distinction causes ferroelectric ceramics, which usually possess higher T_C and lower heat capacity [1,3,5], to display much smaller ΔS compared with ferroelectric polymers [13,14], even though the ΔT data of ceramics as well as polymers were observed to be comparable [5–9].

Despite the fact that the Maxwell relation given by Eq. (1) and phenomenological thermodynamics could provide almost satisfactory accuracy in most numerical predictions, the actual mechanism underlying EC coupling is neither well understood [1] nor systematically established [5]. Specifically, the phenomenological theory has been repeatedly reported to deviate significantly from experimental observations in the vicinity of T_C [15,6]. Ironically, the EC responses of interest are normally found to peak at temperatures near T_C [1,2,9–13]. Even for an identical system, there are obvious discrepancies between the results calculated from the Maxwell relation and phenomenological theory, which is probably caused by the fact that they neglect both the depolarization effect [8] and thermal losses induced by the inevitable electric hysteresis [10]. More importantly, a number of essential issues concerning the EC effect are yet to be addressed.

(i) Although experimental [5,6] and theoretical [7–9] results have demonstrated desirable EC responses in both ferroelectric and paraelectric phases, significant enhancement of the EC coefficient has only been reported in the paraelectric phase [5,7]. Hence, it is important to know whether the desired EC coupling shows gradual reduction [5] or remains nearly constant [7,14] in a wide temperature range of $T > T_C$.

(ii) In addition to the influence of mechanical boundary conditions [16,18], it is also crucial to determine how the electric boundary conditions [8] and size effect [19] influence the intrinsic EC responses.

(iii) Although ΔT is frequently reported to depend on both the increment and the initial value of applied field [16,20], the universal dependence of EC coefficient on the external electric field remains unclear.

To address these concerns, theoretical investigations beyond the above-discussed Maxwell relation and classic phenomenological thermodynamics are required. It should be emphasized that the "demon energy" employed in first-principles-based atomistic simulations, which governs the effective entropy change associated with a variation in the electric field [7,8], excludes the influence of dielectric permittivity, whose dispersion with temperature has been found to have a strong influence on the calculated EC entropy conversion [21]. Most recently, Valant et al. [5] investigated the EC effect using a lattice model developed based on the mean-field theory. However, this method only yielded satisfactory results in the ferroelectric phase and, due to the highly complex nonlinear free energy and entropy equations, no analytical solution has been found for the EC coefficient in the paraelectric phase. Unfortunately, the physics of the complex EC effect above T_C, which is important for exploration of industrial applications, remains unclear.

In this paper, the above issues in dielectric materials are addressed using LGD thermodynamics and Pauli's master (PM) equation, whose suitability in describing the polarization switching dynamics and temporal polarization fatigue mechanisms has been experimentally confirmed for normal ferroelectric single crystals [22]. In contrast to the existing theoretical results that the peaks of EC responses only occur near T_C, the proposed theory highlights a broad extension of the enormous EC effect above T_C owing to the gradual reduction of polarization correlation length and dielectric permittivity in the relaxor paraelectric phase. This may pave a new pathway to realizing EC-effect-based refrigeration devices with wide cooling spans and high cooling capacities. In order to investigate the effect of depolarization field and relaxor dielectric stiffness on EC properties, the free energy of LGD theory is modified in Section 2 to account for the depolarization effect and domain wall energy. In addition, the PM equation is also applied to EC materials to derive the universal dependence of thermal permittivity dispersion and temporal polarization evolution on the general activation parameters. Subsequently, the analytical results obtained are used to develop the general formulas for the EC coefficient in Section 3. In Section 4, direct comparisons are carried out between our analytical results and existing theoretical and experimental data to illustrate the general suitability of the proposed theory. The main findings and important implications are summarized in Section 5.

2. Incorporation of LGD thermodynamics and Pauli's master equation

It is known that the EC properties associated with the dynamic evolution of the order parameter are driven by the thermodynamic forces derived from the total free energy density (F_{total}) of an EC material. Thus, the F_{total} profile in the framework of LGD thermodynamics is commonly used to model the complicated polarization evolution process. However, due to the great difficulty encountered in obtaining an analytical solution of dynamic polarization in terms of the determining parameters when both the depolarization effect and dielectric permittivity dispersion are accounted for, no such solution yet exists [6,13–16]. The fact that existing models and solutions do not consider the depolarization effect and the influence of dielectric permittivity dispersion may have prevented the establishment of a universal formula for the EC coefficient, and may also be the cause of the apparent loss of their validity on EC coupling in the paraelectric phase. In this section, these two important effects are taken into account based on the LGD-type F_{total} [23,24], i.e.:

$$F_{total} = \frac{\alpha}{2}P^2 + \frac{\beta}{4}P^4 + \frac{g}{2}(\nabla P)^2 - PE_{ext} - \frac{1}{2}PE_{dep} \tag{3}$$

where $\alpha = \kappa(T - T_C)$ and the T-independent β are the coefficients of Landau energy expansion; g represents the gradient coefficient for the Ginzburg energy reflecting the presence of polarization heterogeneities [25]; E_{ext} and E_{dep} denote the component of the external electric field along the polarization orientation and the magnitude of the residual depolarization field, respectively. The gradient effect arising from the domain wall is included here for completeness. In accordance with our recent work [26], the Ginzburg energy can be approximated as $4gP^2/3H^2$ based on the classical kink solution [27] for the variation of polarization across a domain wall, where H denotes the wall width.

In order to correlate the depolarization effect with the dielectric permittivity dispersion for analysis of the EC properties, the following empirical formula is adopted [17,24]:

$$E_{dep} = -n_d(P - q_c)/\varepsilon \tag{4}$$

where ε and q_c represent the dielectric permittivity of background material [23] and the reference polarization due to the compensation density of charges from residual defects and electrodes [17], respectively; n_d can be regarded as a geometric depolarization factor dependent on the aspect ratio of reverted polar domains [17] and EC film thickness [28]; q_c is closely related to the screening properties of the EC film and electrode material. It can be postulated from the Gauss's equation [29], i.e. $\nabla \cdot (P - \varepsilon_0 \nabla \varphi) = q_c$, where ε_0 is the vacuum dielectric constant, that in practical situations all the parameters on the right-hand side of Eq. (4) are mutually coupled, and they are closely related to the imposed electric boundary conditions [17] and the spatial distribution of internal defects [30]. Since the focus of the present work is the dynamic effect of electric poling and temperature variation on EC responses, the influence of charge compensation is assumed to be negligible ($q_c \approx 0$). In addition, Hippel [31] revealed that $n_d = 1/3$ for spherical domains. However, $1/n_d$ is found to increase quadratically with the length/diameter ratio of the cylindrical domain [17]. Hence, it can be deduced that the depolarization field in a flat ferroelectric domain is much larger than that of a slender domain. It should be emphasized that the specific size and shape of a domain are significantly affected by the electrical and mechanical boundary conditions, e.g. the interfacial misfit-strain, the intrinsic extrapolation length for polarization and the thickness of the "depleted ferroelectric layer" [32] appearing near the EC film surface or film–electrode interfaces. Further, ε is temperature dependent due to thermodynamic considerations of intrinsic lattice vibrations [25] as well as extrinsic domain patterns or thermal domain wall motion/pinning [28].

So far, a large number of the EC materials exhibit diffuse phase transition and broad dielectric dispersion [33] due to short-range fluctuations [34] of their relaxor [5] or dipolar [14] structures. In general, unconstrained bulk relaxor ferroelectrics possess intrinsic characteristics of a discontinuous first-order transition (FOT), which can be tuned to a continuous second-order transition (SOT) by applying a large electric field [13] or imposing a perfect interfacial misfit strain [16]. In the case of a thin EC film, which is either sandwiched between top and bottom electrodes or deposited on a nonpolar substrate, the main effects of internal stress and substrate lateral clamping include: (i) a simultaneous increase in the magnitude of the dielectric permittivity and a decrease in the sensitivity to temperature [35]; (ii) in increase in the inhomogeneity of the material and its gradient energy; (iii) modification of the energy coefficients in Eq. (3) or even alteration of the sign of β [20], such that during heating the declining rate of order parameter is reduced via transformation of the phase transition order from FOT ($\beta < 0$) to SOT ($\beta > 0$). It is expected that these effects essentially lead to the results obtained by Akcay el al. [20], i.e. imposition of appropriate interfacial clamping condition could reduce the magnitude of EC cooling power and augment to some extent its thermal stability. In the present study, the influences of interfacial/internal stress are neglected and only the EC responses arising from electric poling and thermal activation are considered.

Since in practice an ultrahigh applied electric field plays a crucial role [6] in achieving extraordinary EC responses, the phase transition in EC relaxor ferroelectrics is regarded as a SOT. Subsequently, the paraelectric phase, which consists of many elementary polar nanoregions (PNRs) [14,36] in the absence of an electric field, is assumed to grow into a ferroelectric monodomain (FMD) [20,36] once a critical nucleus of volume V^* is formed in the nonpolar matrix under an applied field [11,22]. Based on the above considerations, it seems reasonable to treat the whole EC film as an ensemble of independent [37] or weakly coupled [5]

PNRs in the absence of external fields, misfit strains and thermal fluctuations, as assumed by Zhukov et al. [37] in discussing their inhomogeneous polarization switching mechanism.

According to Burns and Dacol [38], the average transition temperature of PNRs (T_{PNR}) can be hundreds of degrees higher than the bulk Curie temperature. This would allow us to describe the polarization dependence on the temperature and applied field in the paraelectric phase (above bulk T_C) over a broad temperature range. In view of the weak-interaction nature of PNRs, we could extract the EC coefficient of bulk relaxors based on the transition of one representative PNR into its corresponding FMD. Substituting Eq. (4) and the known Ginzburg energy into the free energy density of the elementary PNR/FMD given by Eq. (3) yields a modified quadratic coefficient of the LGD energy expansion as follows:

$$\alpha^* = \kappa(T - T_{PNR}) + n_d/\varepsilon + 8g/3H^2 \tag{5}$$

Since T_{PNR} is always greater than the temperature of interest, which can be higher than T_C by tens of Kelvin, at a specific temperature the spontaneous polarization for the representative FMD is obtained by minimizing its E_{ext}-free total energy density as:

$$P_{FMD} = \sqrt{\frac{1}{\beta}\left[\kappa(T_{PNR} - T) - \frac{n_d}{\varepsilon} - \frac{8g}{3H^2}\right]} \tag{6}$$

Eq. (6) indicates that the existence of an intrinsic depolarization field and domain wall could considerably decrease the FMD spontaneous polarization, thus giving rise to localized EC responses of FMDs and PNRs. It should be emphasized that, in the case of $E_{ext} = 0$, two stable states of order parameter, i.e. $P_\uparrow$ and $P_\downarrow$ for the polarization vector parallel and reversed-parallel to the applied electric field, respectively, are occupied by the representative FMD with equal occupational probability ($OP_\uparrow = OP_\downarrow$ and $OP_\uparrow + OP_\downarrow = 1$) at T_{PNR}. This leads to the annihilation of the net polarization magnitude (P_{EC}) statistically over the entire EC film among FMDs at temperatures higher than T_{PNR}. However, P_{EC} is positive for either $E_{ext} \neq 0$ or cooling from T_{PNR} because only one polarization state ($P_\uparrow$) is allowed to dominate ($OP_\uparrow > OP_\downarrow$) in minimizing the total energy. For every FMD in which the order parameter is assumed to be uniformly distributed in the polarization form of $P_\uparrow$ and $P_\downarrow$, the minimum energy barrier (F_b) required to activate the polarization switching between $P_\uparrow$ and $P_\downarrow$ is the total energy difference of these two stable polarization states, i.e.:

$$F_b = 2V^* \times P_{FMD} \times E_{ext} \tag{7}$$

Eq. (7) shows that F_b peaks at the largest V^*, corresponding to where lattice symmetry breaking can be observed [39], and that the diffuseness of the relaxor phase transition may originate from the widespread nature of the temperature effect on evolution of V^*. This is consistent with the results of both mean-field theory and transmission electron microscopy observation [25], which indicate that the diffuseness of dielectric response in $Pb(Mg,Nb)O_3$ crystals is characterized by a continuous distribution of the localized polarization correlation volume.

In general, the temporal evolution of $OP_\uparrow$ and $OP_\downarrow$ for PNRs formed in the EC material is governed by the PM equation [22,40], i.e.:

$$\begin{cases} d(OP^\uparrow)/dt = f\left(OP^\downarrow - e^{u_B} \times OP^\uparrow\right) \\ d(OP^\downarrow)/dt = f\left(e^{u_B} \times OP^\uparrow - OP^\downarrow\right) \end{cases} \tag{8}$$

where $u_B = F_b/kT$ and k is Boltzmann's constant; f denotes the intrinsic relaxation frequency at T_{PNR}, which has been found to have no significant role in determining the equilibrium (in the limit of time $t \to \infty$) $OP_\uparrow = 1/(1 + e^{-u_B})$ and $OP_\downarrow = 1/(1 + e^{u_B})$ [22]. Under the activation of either E_{ext} or T, by assuming that all the FMDs/PNRs in the EC film possess identical maxima for their saturated polarization, P_{sat}, on the whole the statistical value of P_{EC} subjected to variation of u_B can be deduced by weighting the localized order parameter among the entire sample of FMDs/PNRs with their equilibrium occupational probabilities, i.e.:

$$P_{EC} = P_{sat}\frac{1 - \exp(-u_B)}{1 + \exp(-u_B)} \tag{9}$$

in which P_{EC} should be along the direction of E_{ext}. It is important to note that u_B, which directly integrates the activations from E_{ext} and external cooling, is closely related to the governing parameter of "demon energy" employed in the first-principles calculations that govern the variation of entropy [7,8]. Eqs. (7) and (9) imply that, in addition to T and E_{ext}, the variation of V^* is also expected to play an equally vital role on the EC response accompanied by variations in polarization. Furthermore, we can utilize Eq. (9) to extract dielectric dispersion in terms of temperature. Since less than 10% reduction of bulk spontaneous polarization is actually attributed to the effects of depolarization [22] and domain walls [41], the temperature-driven dielectric dispersion can be deduced based on the assumption of temperature-independent domain wall width.

2.1. Case I. Dielectric response in ferroelectric phase ($T < T_C$)

In the temperature range below T_C, in which the material is in the ferroelectric state, the magnitude of saturated polarization will deviate from Eq. (6) in the presence of E_{ext}. In this case, the approximation $P_{sat} = P_{FMD} + \Delta P = P_{FMD} + \varepsilon E_{ext}$ is commonly adopted to estimate the average dielectric effect with respect to E_{ext} [17]. Most importantly, the validity of Eq. (9) for EC materials requires the constraint $\varepsilon = \partial P_{EC}/\partial E_{ext}$ be strictly satisfied over a wide u_B range, which gives rise to the temperature-induced incremental ratio of EC film polarization as follows:

$$\frac{\Delta P}{P_{FMD}} = \frac{u_B}{1 - u_B + e^{-u_B}} \tag{10a}$$

Since $\Delta P = \varepsilon E_{ext}$, Eq. (10a) indicates the thermal dispersion of dielectric properties of EC materials, which is crucial for characterization of the EC responses through tuning the magnitude of the depolarization field given by Eq. (4).

2.2. Case II. Dielectric response in high-temperature paraelectric phase ($T_C \leqslant T \leqslant T_{PNR}$)

In view of the fact that $P_{sat} \approx P_{FMD}$ in the weakly interactive paraelectric phase, the application of E_{ext} will merely revert or redistribute the polarization direction of FMD/PNR. By differentiating the P_{EC} of EC film with respect to E_{ext} and solving $\varepsilon = \partial P_{EC}/\partial E_{ext}$, we obtain:

$$\frac{\Delta P}{P_{FMD}} = \frac{2u_B}{2 + e^{-u_B} + e^{u_B}} \tag{10b}$$

Our plots for the inverse functions of Eqs. (10a) and (10b) vs. $1/u_B$ (not shown here) show that the temperature-dependent $1/\varepsilon$ curve is composed of two nearly straight lines intersecting at a critical u_B value which corresponds to the Curie temperature. This result is in agreement with Curie–Weiss law, in which ε^{-1} is linearly proportional to $|T - T_C|$ over a broad temperature range. In addition, the ε in the ferroelectric phase is found to diverge at $u_B = 1.278$, whereas that of the paraelectric phase peaks at $u_B = 1.543$. Since u_B decreases with increasing temperature, these findings seem to explain the well-known size effect on T_C, i.e. that the smaller the size of nanoscale polar material, the lower is its Curie temperature. Thus, we can infer that Eqs. (10a) and (10b) are able to reflect the dielectric permittivity diffusivity of the EC material.

As the framework of this work lies within the concept of the "superparaelectric" nature of commonly used EC materials [25] and the focus is on their EC responses above T_C, we limit our derivations and discussions to the case of ε in the paraelectric phase, which is given by Eq. (10b). Subsequently, a modified dielectric stiffness, $\kappa^* = \partial\alpha^*/\partial T$, taking into account the effect of broad dielectric dispersion during diffuse transition of relaxor, can be obtained:

$$\kappa^* - \kappa = \frac{k}{4\beta V^* P_{FDM}^2}\left(2 + e^{-u_B} + e^{u_B} + u_B e^{-u_B} - u_B e^{u_B}\right) \tag{11}$$

Eqs. (10) and (11) show that the dielectric stiffness is significantly enhanced at elevated temperatures due to the augmented depolarization effect. Although in general the depolarization effect appears to have insignificant influence on the dynamics of ferroelectric domain reversal, the following points are worth noting. (i) Since the screening length of electrodes or the thickness of the grain boundary and the "depleted" ferroelectric layer is not smaller than the critical PNR dimensions of interest, the depolarization field given by Eq. (4) would provide an energy barrier and, thus, substantially affect V^*. (ii) In reality, the gradual reduction of V^* with increasing temperature will inevitably decrease u_B and increase $k/2\beta V^* P_{FDM}^2$, which in turn raises κ^* and the EC responses. This type of thermal reinforcement is vital for understanding the large enhancement of dielectric stiffness with an increase in temperature [14].

In order to describe more precisely the EC properties in dielectric materials, especially at temperatures above T_C, Eqs. (10) and (11) must be able to describe accurately the broad diffuse nature of the transition as well as the dispersion of dielectric permittivity dispersion over a wide range of T and E_{ext}. Thus, it is important to check the effectiveness of Eqs. (10) and (11) before further discussion on the theory of EC responses.

The suitability of Eq. (10) is examined using the recently investigated lead-free $SrBi_2Ta_2O_9$ (SBT) thin film [10]. Fig. 1a shows that the diffusivity of SBT dielectric permittivity determined from Eq. (10b) is in perfect agreement with the corresponding experimental data obtained by Chen et al. [10] over a broad temperature range of at least 200 K. Fig. 1b shows both the mean-theory solution, in which the net polarization of ferroelectric nanocomposite decreases almost linearly with increasing temperature [25], and the existing experimental results, in which the curve of temperature-induced polarization exhibits an upward convex deviation from the mean-theory result [9,10]. The convex feature of the $P_{FMD} \times V^*$ curve is probably the consequence of an initial gradual growth followed by subsequent faster reduction of V^* during the process of heating up. This is because the values of V^* at temperatures far from T_C are much smaller due to a lower degree of lattice symmetry breaking at these temperatures compared to that near T_C. It is also important to note that the identical slope of the black solid line and the long pink dashed line shown in Fig. 1b indicates a stable and small magnitude of polarization correlation length at temperatures far from T_C, while the asymmetric variation of V^* in the vicinity of T_C is similar to the distribution of local polarization correlation volume calculated from the mean-field theory [25]. These distinct features are useful for explaining the asymmetric nature of the relaxor's diffuse transition [36,42]. It is noteworthy that the as-shown V^* evolution in Fig. 1b is in remarkable agreement with the recent results obtained by Glinchuk et al. [43] for variation of correlation radius in thin ferroelectric films.

Eq. (11) extends the classic phenomenological theory in which an assumption of time independence was used to establish the solutions for dielectric stiffness [3,19]. However, this assumption has encountered some challenges [14]. Apart from the unsatisfactory accuracy in simulating temperature-dependent properties of typical relaxor ferroelectrics, the predicted EC response based on the LGD theory significantly underestimates ΔT in $BaTiO_3$ multilayer [6] and ΔS in P(VDF–TrFE–CFE) thin films [14]. In contrast, the calculated values of κ^* from Eq. (11) are in excellent agreement with the temperature-driven dielectric stiffness EC enhancement observed by Neese et al. [14], as shown in Fig. 2. Therefore, it is encouraging to further

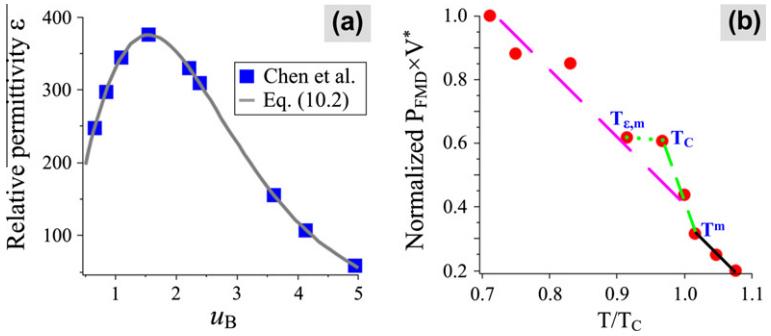

Fig. 1. (a) Comparison of the predicted dielectric permittivity of $SrBi_2Ta_2O_9$ thin film from Eq. (10b) and experimental data [10]. (b) Theoretical prediction of the asymmetric distribution of the normalized product of $P_{FMD} \times V^*$ in the same temperature range as that of (a). The black solid line in parallel with the long pink dashed line indicates nearly the same linear reduction of spontaneous polarization, while the green dotted line and short-dashed line illustrate the asymmetric dispersion of V^* in the vicinity of T_C. The Curie temperature is $T_C = 561$ K, and $T_{\varepsilon,m}$ and T^m are temperatures corresponding to the peak of dielectric permittivity and the maximum derivative of $P_{FMD} \times V^*$ with respect to temperature, respectively. (For interpretation of the references to color in this figure legend, the reader is referred to the web version of this article.)

analyze the EC response based on the inferences obtained from the PM equation.

3. Analytical investigation on EC responses

In view of the analytical expressions derived in the previous section, the electric responses of EC films in terms of polarization induced by the activating effect of temperature and applied electric field is bound to be governed by Eq. (9), in which the saturated polarization is approximated as P_{FMD} given by Eq. (6), which is temperature governed. Hence, we could insert $\gamma_E = \partial P_{EC}/\partial T$ into the Maxwell relation given by Eq. (2) to obtain the EC coefficient:

$$(\chi)_S C_E = \frac{2u_B P_{FMD}}{2 + e^{-u_B} + e^{u_B}} - T\left(\frac{\partial P_{FMD}}{\partial T}\right)\frac{1 - e^{-2u_B} + 2u_B e^{-u_B}}{(1 + e^{-u_B})^2} \quad (12)$$

where the subscripts S and E denote the condition of constant entropy and constant E_{ext}, respectively. The first term on the right-hand side of Eq. (12) represents the contribution from relaxor dielectric dispersion (compare Eqs. (10) and (12)), while the second term is mainly attributed to the strong coupling between the intrinsic pyroelectric effect however, the dielectric stiffness enhancement driven by either the increased E_{ext} or environmental heating. In view of the fact that the dielectric dispersion and pyroelectric response are normally material properties of a relaxor, the only feasible approach to enhance the EC effect is to increase either the electric polarization or the magnitude and sensitivity of dielectric stiffness with respect to T and E_{ext}. Note that the temperature T^m, at which the maximum derivative of dielectric permittivity with respect to temperature occurs, has been shown both experimentally (see Fig. 1b) and theoretically [44] to be higher than T_C of the commonly used relaxors. We can thus postulate that the measured temperature T^{opt} is slightly larger than T_C, as commonly observed.

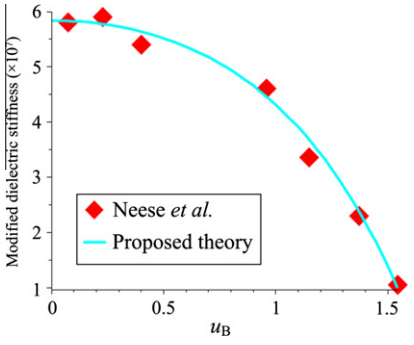

Fig. 2. Comparison of predictions from Eq. (11) with the experimental data for the temperature-dependent dielectric stiffness of P(VDF–TrFE–CFE) thin film extracted from Ref. [14]. On decreasing u_B, the diamonds denote the measured stiffness in the temperature range of 30–60 °C and 90–110 °C at increments of 10 °C.

Furthermore, by combining Eqs. (6), (10) and (11), we obtain:

$$\partial P_{FMD}/\partial T = -\kappa^*/(2\beta P_{FMD}) \quad (13)$$

Substituting Eq. (13) into Eq. (12) yields two formulas for χ, i.e. the EC coefficient at constant electric field, $\chi(u_B)_E$, which changes with the variation of T, and that at constant T, $\chi(u_B)_T$, which changes with E_{ext}. Note that u_B includes both kinds of direct activation arising from E_{ext} and T, and is, therefore, a more general parameter. It can be shown that χ consists of three components, each of which has a unique interpretation; and three superscripts, I, II and III, are used to differentiate them in $\chi(u_B)_T$ and $\chi(u_B)_E$ as follows:

$$\chi(u_B)_E C_E = P_{FMD} \times \chi^{\mathrm{I}}(u_B)_E + \frac{2\kappa E_{ext} V^*}{k\beta}\chi^{\mathrm{II}}(u_B)_E + \frac{n_d E_{ext}}{2\beta^2 P_{FMD}^2}\chi^{\mathrm{III}}(u_B)_E \quad (14)$$

$$\chi(u_B)_T C_E = P_{FMD} \times \chi^{\mathrm{I}}(u_B)_T + \frac{\kappa T}{\beta P_{FMD}}\chi^{\mathrm{II}}(u_B)_T + \frac{n_d kT}{4V^*\beta^2 P_{FMD}^3}\chi^{\mathrm{III}}(u_B)_T \quad (15)$$

where

$$\begin{cases} \chi^{\mathrm{I}}(u_B)_E = \chi^{\mathrm{I}}(u_B)_T = \frac{2u_B}{2+e^{-u_B}+e^{u_B}} \\ u_B\chi^{\mathrm{II}}(u_B)_E = \chi^{\mathrm{II}}(u_B)_T = \frac{1-e^{-2u_B}+2u_Be^{-u_B}}{2(1+e^{-u_B})^2} \\ \frac{\chi^{\mathrm{III}}(u_B)_E}{\chi^{\mathrm{II}}(u_B)_E} = \frac{\chi^{\mathrm{III}}(u_B)_T}{\chi^{\mathrm{II}}(u_B)_T} = (2+e^{-u_B}+e^{u_B}+u_Be^{-u_B}-u_Be^{u_B}) \end{cases} \quad (16)$$

Eq. (14) shows that in the case of constant E_{ext} and n_d, the heating-driven decrease in polarization (refer to Eq. (6)) enhances quadratically the proportion of $\chi^{\mathrm{III}}(u_B)_E$ and, simultaneously, reduces proportionally that of $\chi^{\mathrm{I}}(u_B)_E$. This is consistent with the mechanisms recently conjectured by Neese et al. [14] to explain the distinct temperature-driven EC responses in terms of ΔS and ΔT in quenched and annealed P(VDF–TrFE–CFE). In addition, Eq. (14) also infers that a proportional increase in the EC coefficient is produced by the increase in n_d, which agrees with the proportional decrease in χ due to the improvement in the screening parameter [8]. Fig. 3a shows that, compared to a monotonously increasing $\chi^{\mathrm{II}}(u_B)_E$ during heating, $\chi^{\mathrm{I}}(u_B)_E$ shows a significant increase over a narrow temperature range followed by a slow decline, and that before $\chi^{\mathrm{I}}(u_B)_E$ reaches its peak, the rapid appearance and increase of $\chi^{\mathrm{III}}(u_B)_E$ at higher temperature strongly enhances the overall EC coefficient $(\chi)_E$. It should be emphasized that the EC enhancement due to both $\chi^{\mathrm{II}}(u_B)_E$ and $\chi^{\mathrm{III}}(u_B)_E$ only takes place at relatively high temperatures. To the best of our knowledge, this is the first direct analytical demonstration of both the significant enhancement of EC effect in the paraelectric phase and its broad effective temperature range, as confirmed by the experimental observations [5,6], first-principles simulations [7] and modified Ising model [4]. In addition, these findings may help identify some polarizable materials with T_C lower than room temperature (RT), enabling enhanced EC responses near RT, which will be critical for solid-state refrigeration. A typical example in this direction is the recently reported $(Ba_{0.5}Sr_{0.5})TiO_3$ thin film [7]. It is most interesting that an optimum temperature, T^{opt}, for the maximum $(\chi)_E$ does exist, which is expected since all the derivatives of the three terms in $(\chi)_E$ are mutually canceled out, as shown in Fig. 3b.

The E_{ext}-activated variations of $\chi^{\mathrm{I}}(u_B)_T$, $\chi^{\mathrm{II}}(u_B)_T$ and $\chi^{\mathrm{III}}(u_B)_T$ under fixed temperature is demonstrated in Fig. 3c. It can be seen that while $\chi^{\mathrm{I}}(u_B)_T$ and $\chi^{\mathrm{II}}(u_B)_T$ exist over the whole temperature range, $\chi^{\mathrm{III}}(u_B)_T$ only exists over a short range at higher temperatures, as implied by Eq. (15). Note that if an ultrahigh E_{ext} is applied, there is a possibility that the enhancement of χ near T^{opt} may be reduced, as probably implied in the work by Lisenkov and Ponomareva [7] for $E_{ext} > 90$ MV m^{-1}. Hence, in addition to the primary limitation from the electric breakdown strength of EC relaxors [1,20], the E_{ext} employed to realize EC coupling enhancement should not exceed the critical value for maximizing $\chi^{\mathrm{III}}(u_B)_T$, as shown in Fig. 3c.

In practice, both T and E_{ext} are likely to change simultaneously due to nonuniform thermal conduction and intrinsic relaxor inhomogeneity. The generality of u_B and Eqs. (12)–(16) should be examined in order to analyze EC coupling in the presence of such complications. The variations of the three components of χ and their sum with respect to u_B are presented in Fig. 3d. It can be seen that the competition between the slow decrease of relaxor

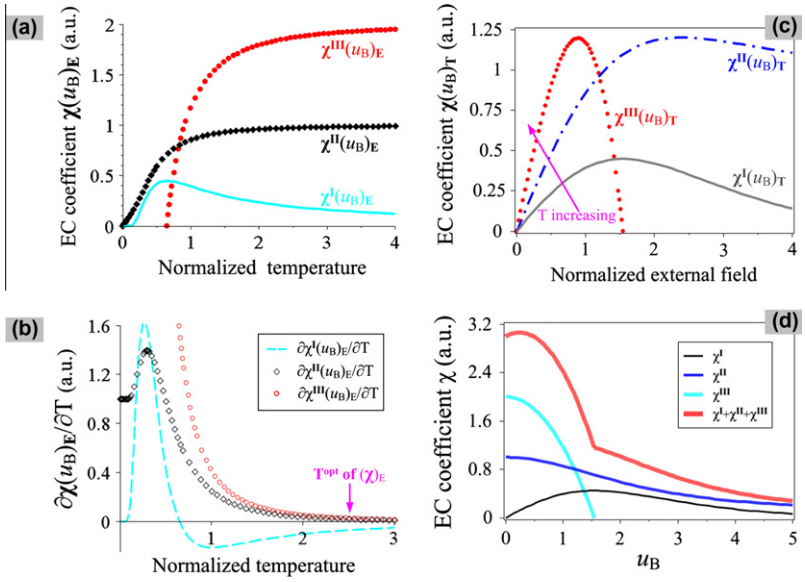

Fig. 3. Temperature-dependent variations (at constant applied field) of (a) the three component functions of the EC coefficient χ and (b) their derivatives with respect to temperature. The arrow in (b) indicates the optimum temperature T^{opt}, at which the sum of the three terms in $(\chi)_E$ is maximized since their net derivative is zero. (c) E_{ext}-driven variation of the three component functions at constant temperature. The arrow in (c) points to the direction of increasing temperature, indicating that $(\chi^{\mathrm{III}})_T$ is only effective at higher temperatures and that $(\chi^{\mathrm{I}})_T$ and $(\chi^{\mathrm{II}})_T$ exist over a relatively larger range of T compared with that of $(\chi^{\mathrm{III}})_T$. (d) Variations of the three χ components and their sum, activated by changes of both T and E_{ext}, with respect to u_B.

dielectric dispersion and the steep increase of dielectric stiffness results in the existence of an optimum u_B, which occurs at T^{opt}. It is noteworthy that such an optimal u_B could be easily tuned by controlling the grain size of ferroelectric ceramics [19], since decreasing the grain size is an effective method for enhancing dielectric permittivity [45]. The existence of an optimum u_B suggests that T and E_{ext} can be controlled to yield better EC responses, and that more accurate management of the internal heat transfer in EC materials could be used to achieve the commercially required EC responses and cooling power.

4. Results and discussion

Although the first study of the EC effect in Rochelle salt [46] can be traced back to 1930s, direct measurements of enormous EC response in relaxors were not available until very recently [5,6]. To examine the versatility of the analytical formulas established in Section 3, the $(Ba_{0.5}Sr_{0.5})TiO_3$ (BST) alloy [7] is selected for theoretical study of the EC effect at the room temperature, which will be compared with the experimental results obtained for the $0.92Pb(Zn_{1/3}Nb_{2/3}O_3)$–$0.08PbTiO_3$ (PZN-PT) thin film [5]. Direct comparison of the existing ΔT data (see Refs. [1–9,20]) shows a similar trend in the variation of ΔT over a wide temperature range in various EC materials. Fig. 4 shows that the variation of EC coefficient with respect to temperature obtained from theoretical predictions using Eq. (14) is in excellent agreement with first-principles calculation for BST [7]. The slight deviation at 240 K is probably due to our simplistic selection of temperature-independent critical volume and constant proportions for the three components of χ. On one hand, on heating, the critical volume should decrease continuously at temperatures between T_C and T^m, as demonstrated in Fig. 1b, which leads to an overestimation of χ at lower temperatures such that the decreasing trend of χ at higher temperatures can be well described. On the other hand, the mentioned proportions should be temperature dependent, and our assumption of the reverse will increase the extent of enhancement, and thus results in prediction of a larger χ.

The fitting results of Fig. 4 reveal that the factors associated with $\chi^{I}(u_B)_E$ and $\chi^{II}(u_B)_E$ are of the same order for the simulated $(Ba_{0.5}Sr_{0.5})TiO_3$ alloy, and thus yield an estimation of its V^* as being proportional to $\beta k P_{FMD}/\kappa E_{ext}$. In view of the lack of the necessary data for $(Ba_{0.5}Sr_{0.5})TiO_3$, the estimation of V^* is made based on the corresponding data of $Ba_{2.2}Sr_{0.8}Ta_2O_9$ [47], i.e. $\beta = 3.75 \times 10^9$, $\kappa = 2.03 \times 10^5$ and $P_{FMD} = 15.5\ \mu C\ cm^{-2}$. By setting the applied field $E_{ext} = 100\ kV\ cm^{-1}$ [7], a critical domain volume of $V^* \approx 5.6\ nm^3$ is determined, which corresponds to the smallest in-plane length of 24.2 Å for a rectangular domain of about six lattice units when its length/thickness ratio is selected as 2.5 [48], and corresponds to a critical out-of-plane length of 2.12 nm in the case of a conic domain if the length/radius ratio is chosen to be 4/3 [49]. These results are in excellent agreement with the critical thickness of about 2.4 nm for ferroelectricity in perovskite (e.g. $BaTiO_3$) ultrathin films [50], as well as the domain-wall width of several lattices as measured by atomic force microscopy [51].

Fig. 5 presents the variations of EC temperature change and coefficient with respect to applied electric field obtained from Eq. (15), first-principles calculations for BST thin film at 200 and 285 K (extracted from Ref. [7]), and direct measurement of χ in PZN-PT crystal at 453 K (extracted from Ref. [5]). It is obvious that a linear approximation of χ at high E_{ext} is valid, as predicted by Eq. (15) (see Fig. 3c). The two χ curves for two different temperature ranges, one below and the other above T_C [7], are in excellent agreement with our analytical results. When E_{ext} is comparable with the intrinsic coercive field (E_C), linear approximation is no longer valid, as shown in the nascent activation stage (left of the hollow arrow in Fig. 5), and an exponentially activated increase [52] will give a better representation. In this case, the original E_{ext} has to be modified as $E_{ext}-E_C$ so that the

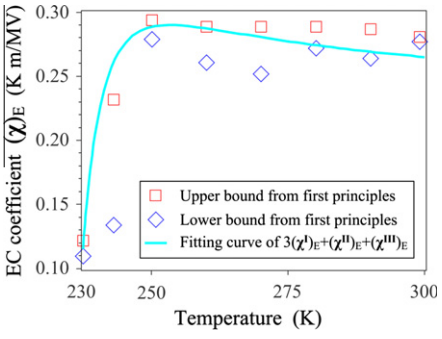

Fig. 4. Variation of EC coefficient with respect to temperature predicted by Eq. (14) and from first-principles calculations for $(Ba_{0.5}Sr_{0.5})TiO_3$ [7]. The upper and lower bound at each T are the maximum and minimum values, respectively. The Curie and optimum temperature are taken to be 230 and 250 K, respectively.

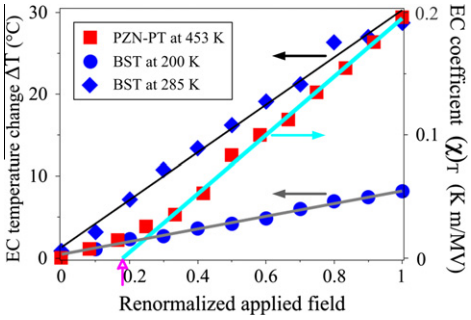

Fig. 5. Variations of EC temperature change and coefficient with respect to applied electric field from Eq. (15), first-principles calculations for BST thin film at 200 K and 285 K [7], and direct measurement of χ in PZN-PT (110) crystal at 453 K [5]. The solid lines are the predictions from Eq. (15). The largest applied fields are 1.2 and 100 MV m^{-1} for PZN-PT crystal and BST alloys, respectively. The hollow arrow indicates our predicted coercive field of 0.215 MV m^{-1} for the PZN-PT crystal. The BST data at 200 and 285 K are first-principles calculations for temperatures between 190 and 210 K as well as 270 and 300 K, respectively, obtained from Ref. [7].

nonequilibrium effect dominated by the dynamic motion of ferroelectric domain walls [53] can be included in the proposed theory. This type of modification provides a good explanation for the slight rightward shift of our predicted line with respect to the origin of the coordinate system in Fig. 5. It is important to note that our result of $E_C = 0.215\ \mathrm{MV\ m^{-1}}$ lies in the measured range of 0.2–0.3 $\mathrm{MV\ m^{-1}}$ for PZN-PT single crystals [5].

The results of the present study, which are obtained using a combination of PM equation, classic LGD thermodynamics and the appropriate Maxwell relation, present the dielectric and EC properties of stress-free polarizable materials under electric poling and temperature change. The proposed approach offers an excellent interpretation, by incorporating the microscopic thermal evolution of correlation length, of the recently observed enhancement in EC responses, and seems capable of remedying the apparent loss of validity, especially in the temperature range near and above Curie point, of the existing widely employed theories, such as the classic phenomenological theory and the recently proposed lattice model based on the mean-field theory. It is found that by applying a sufficiently high electric field, the EC material with larger dielectric stiffness and smaller correlation length could extend its enormous EC effect above the Curie temperature. Furthermore, the above-mentioned enhancement of the EC effect above T_C is essentially attributed to the thermal reduction of dielectric permittivity and correlation length. This finding may provide a new and effective way to tune the extent of enhancement, such as by engineering the first derivative of dielectric permittivity with respect to temperature via controlling the grain size of relaxor ceramics [19,54], by fabricating ultrathin ferroelectric films [35] and initializing metal–insulator transition [44,54], and by manipulating the shape and volume of the initially formed PNRs via applying a nanoscale electric field using scanning probe microscopy tip-voltage [49] and nanoconfining EC thin-films [55,56].

Finally, it should be pointed out that in order to better understand the nature of the EC effect, the following important issues require further consideration.

(i) In the present study, only the equilibrium solution of PM equations is adopted to deduce the dielectric responses and order parameter evolution in EC materials, however, the dependence of permittivity/depolarization-field on the frequency-related dynamic effects and ultrafast domain wall motion [57] could be crucial.
(ii) The complicated dynamics of order parameter in three-dimensional EC devices is influenced by spatially localized charges and defects as well as by electrode material [30,58].
(iii) The effects of extrapolation length and misfit strain, which are neglected in the presently formulated total energy [17], may play a predominant role in determining the depolarization factor and in turn the EC responses of polar nanofilms.

5. Conclusion

In summary, Pauli's master equation has been used to deduce the general dependence of electric polarization on temperature and electric field in relaxor ferroelectric single crystals and polymers, and to study relaxor diffuse phase transition as well as temperature-dependent dielectric stiffness. Both the depolarization effect and dielectric permittivity dispersion have been considered within the framework of the classic LGD thermodynamics and the Maxwell relation in determining the EC coefficient. It has been found that the overall EC coefficient consists of three components: temperature-dependent dielectric dispersion, intrinsic pyroelectric effect, and the enhancement of bulk dielectric stiffness driven by the applied electric field or environmental heating. Moreover, the proportions of these components are strongly dependent on the dynamic evolution of electric polarization and its correlation length, which provides a microscopic explanation for the thermally driven EC enhancement and distinct electrocaloric properties of relaxor and polymer. Therefore, the EC effect can be attributed to either distinct dominant contributions at different activation levels or different electrocaloric materials. The proposed approach improves upon existing theories at temperatures near to or far above the Curie temperature. Finally, our analysis suggests a way to utilize the dielectric permittivity and correlation volume of EC materials as a tool to tune the enhancement of the EC coefficient.

Acknowledgements

Research Grants Council of the Hong Kong Special Administrative Region, under Project No. HKU 716508E, is acknowledged. We would like to thank Professor Huajian Gao at Brown university for his thought-provoking comments and discussion.

References

[1] Mischenko AS, Zhang Q, Scott JF, Whatmore RW, Mathur ND. Science 2006;11:1270.
[2] Neese B, Chu BJ, Lu SG, Wang Y, Furman E, Zhang QM. Science 2008;321:821.
[3] Lu SG, Zhang QM. Adv Mater 2009;21:1983.
[4] Cao HX, Li ZY. J Appl Phys 2009;106:094104.
[5] Valant M, Dunne LJ, Axelsson AK, Alford NM, Manos G, Peräntie J, et al. Phys Rev B 2010;81:214110.
[6] Bai Y, Zheng GP, Shi SQ. Appl Phys Lett 2010;96:192902.
[7] Lisenkov S, Ponomareva I. Phys Rev B 2009;80:140102. R.
[8] Prosandeev S, Ponnareva I, Bellaiche L. Phys Rev B 2008;78:052103.
[9] Liu PF, Wang JL, Meng XJ, Yang J, Dkhil B, Chu JH. New J Phys 2010;12:023035.
[10] Chen H, Ren TL, Wu XM, Yang Y, Liu LT. Appl Phys Lett 2009;94:182902.
[11] Correia TM, Young JS, Whatmore RW, Scott JF, Mathur ND, Zhang Q. Appl Phys Lett 2009;95:182904.
[12] Mischenko AS, Zhang Q, Scott JF, Mathur ND. Appl Phys Lett 2006;89:242910.
[13] Li B, Ren WJ, Wang XW, Meng H, Liu XG, Wang ZJ, et al. Appl Phys Lett 2010;96:102903.

[14] Neese B, Lu SG, Chu BJ, Zhang QM. Appl Phys Lett 2009;94:042910.
[15] Guyomar D, Sebald G, Guiffard B, Seveyrat L. J Phys D: Appl Phys 2006;39:4491.
[16] Akcay G, Alpay SP, Rossetti GA, Scott JF. J Appl Phys 2008;103:024104.
[17] Zheng Y, Woo CH, Wang B. Nano Lett 2008;8:3131.
[18] Qiu JH, Jiang Q. J Appl Phys 2008;103:084105.
[19] Qiu JH, Jiang Q. J Appl Phys 2009;105:034110.
[20] Akcay G, Alpay SP, Mantese JV, Rossetti GA. Appl Phys Lett 2007;90:252909.
[21] Zhu XH, Guigues B, Defaÿ E, Aïd M. J Appl Phys 2008;104:074118.
[22] Vopsaroiu M, Blackburn J, Cain MG, Weaver PM. Phys Rev B 2010;82:024109.
[23] Ma DC, Zheng Y, Woo CH. Appl Phys Lett 2009;95:262901.
[24] Uchino K. Ferroelectric devices. New York: CRC Press; 2010 [chapter 4]. Grindlay J. An introduction to the phenomenological theory of ferroelectricity. Oxford: Pergamon Press; 1970.
[25] Li S, Eastman JA, Newnham RE, Cross LE. Phys Rev B 1997;55:12067.
[26] (a) Shi YP, Soh AK. EPL 2010;92:57006;
(b) Shi YP, Soh AK, Weng GJ. J Appl Phys 2011;109:024102.
[27] Falk F. Z Phys B 1983;51:177.
[28] Tagantsev AK, Gerra G. J Appl Phys 2006;100:051607.
[29] Xiao Y, Shenoy VB, Bhattacharya K. Phys Rev Lett 2005;95:247603.
[30] Wang D, Wang YZ, Zhang Z, Ren XB. Phys Rev Lett 2010;105:205702.
[31] Hippel AV. Rev Mod Phys 1950;22:221.
[32] (a) Wang Y, Niranjan MK, Janicka K, Velev JP, Zhuravlev MY, Jaswal SS, et al. Phys Rev B 2010;82:094114;
(b) Dawber M, Scott JF. Appl Phys Lett 2000;76:1060;
(c) Dawber M, Scott JF. Appl Phys Lett 2000;76:3655;
(d) Scott JF. Ferroelectric memories. Berlin: Springer Verlag; 2000.
[33] Viehland D, Jang SJ, Cross LE, Wuttig M. Phys Rev B 1992;46:8003.
[34] Scott JF. ChemPhysChem 2010;11:341.
[35] Ponomareva I, Bellaiche L, Resta R. Phys Rev Lett 2007;99:227601.
[36] Bobnar V, Kutnjak Z, Pirc R, Blinc R, Levstik A. Phys Rev Lett 2000;84:5892.
[37] Zhukov S, Genenko YA, Hirsch O, Glaum J, Granzow T, Seggern HV. Phys Rev B 2010;82:014109.
[38] Burns G, Dacol F. Phys Rev B 1983;28:2527.
[39] Vojta M. Adv Phys 2009;58:699.
[40] Kreuzer HJ. Nonequilibrium thermodynamics and its statistical foundations. Oxford: Oxford University Press; 1981 [chapter 10].
[41] Aravind VR, Morozovska AN, Bhattacharyya A, Lee D, Jesse S, Grinberg I, et al. Phys Rev B 2010;82:024111.
[42] Noblanc O, Gaucher P, Calvarin G. J Appl Phys 1996;79:4291.
[43] Glinchuk MD, Morozovska AN, Eliseev EA. Ferroelectrics 2010;400:243.
[44] Lu ZG, Calvarin G. Phys Rev B 1995;51:2694.
[45] Ihlefeld JF, Borland WJ, Maria JP. Adv Mater 2007;17:1119.
[46] Kobeko P, Kurtschatov J. Z Phys 1930;66:192.
[47] Tanaka M, Hironaka K, Onodera A. Ferroelectrics 2002;266:103.
[48] Stachiotti MG, Sepliarsky M. Phys Rev Lett 2011;106:137601.
[49] Shi YP, Hong L, Soh AK. J Appl Phys 2010;107:124114.
[50] Junquera J, Ghosez P. Nature (London) 2003;422:506.
[51] Shilo D, Ravichandran G, Bhattacharya K. Nat Mater 2004;3:453.
[52] Chen YC, Lin QR, Chu YH. Appl Phys Lett 2009;94:122908.
[53] Morozovska AN, Eliseev EA, Li Y, Svechnikov SV, Maksymovych P, Shur VY, et al. Phys Rev B 2009;80:214110.
[54] Dang ZM, Lin YH, Nan CW. Adv Mater 2003;15:1625.
[55] Kang SJ, Bae I, Choi J-H, Park YJ, Jo PS, Kim Y, et al. J Mater Chem 2011;21:3619.
[56] Kang SJ, Bae I, Shin YJ, Park YJ, Huh J, Park SM, et al. Nano Lett 2011;11:138.
[57] Molotskii M, Rosenwaks Y, Rosenman G. Annu Rev Mater Res 2007;37:271.
[58] Okatan MB, Mantese JV, Alpay SP. Acta Mater 2010;58:39.